

Single-Layer Vision Transformers for More Accurate Early Exits with Less Overhead

Arian Bakhtiarnia, Qi Zhang, *Member, IEEE*, and Alexandros Iosifidis, *Senior Member, IEEE*

Abstract—Deploying deep learning models in time-critical applications with limited computational resources, for instance in edge computing systems and IoT networks, is a challenging task that often relies on dynamic inference methods such as early exiting. In this paper, we introduce a novel architecture for early exiting based on the vision transformer architecture, as well as a fine-tuning strategy that significantly increase the accuracy of early exit branches compared to conventional approaches while introducing less overhead. Through extensive experiments on image and audio classification as well as audiovisual crowd counting, we show that our method works for both classification and regression problems, and in both single- and multi-modal settings. Additionally, we introduce a novel method for integrating audio and visual modalities within early exits in audiovisual data analysis, that can lead to a more fine-grained dynamic inference.

Index Terms—Dynamic inference, early exiting, multi-exit architectures, vision transformers, multi-modal deep learning.

I. INTRODUCTION

OVER the past decade, deep learning has shown tremendous success across various fields, such as computer vision and natural language processing [1]. However, deep learning models are by definition composed of many layers of interconnected neurons, often reaching billions of parameters, which makes them computationally expensive. This has sparked a great deal of research in order to make deep learning models more lightweight, for which many approaches have been proposed, for instance, *model compression* methods [2] such as *quantization* [3], *pruning* [4], *low-rank approximation* [5] and *knowledge distillation* [6], [7].

More and more emerging internet of things (IoT) applications are integrating deep learning models, such as video surveillance, voice assistants, augmented reality and cooperative autonomous driving, which are often time-sensitive and require inputs to be processed within specific deadlines [8]–[10]. The heavy computational burden of deep learning becomes problematic for these time-critical IoT applications, due to resource-constrained IoT devices. Edge Computing is a promising computing paradigm for addressing this issue, in which the deep learning task is offloaded to edge servers in the proximity of IoT devices.

Arian Bakhtiarnia, Qi Zhang and Alexandros Iosifidis are with DIGIT, the Department of Electrical and Computer Engineering, Aarhus University, Aarhus, Midtjylland, Denmark (e-mail: arianbakh@ece.au.dk; qz@ece.au.dk; ai@ece.au.dk).

This work was partly funded by the European Union’s Horizon 2020 research and innovation programme under grant agreement No 957337, and by the Danish Council for Independent Research under Grant No. 9131-00119B. This publication reflects the authors views only. The European Commission and the Danish Council for Independent Research are not responsible for any use that may be made of the information it contains.

Since edge computing systems introduce computation of flooding over a communication network and involve multiple nodes working collaboratively in order to complete the task in a timely manner, transmission time has to be taken into account in addition to the deep learning computation time. However, transmission time may vary greatly over time and across different channels. Consequently, deep learning models running on edge computing systems and IoT networks should be capable of *anytime prediction*, meaning they should be able to provide a valid response even if they are interrupted before traversing the entire neural network, although the model is expected to provide a better answer if it is allowed to run for longer time.

Dynamic inference approaches [11] modify the computation graph based on each input during the inference phase in order to fit the time constraints. A dynamic inference approach that particularly suits anytime prediction is *early exiting* [12], also referred to as *multi-exit architectures* or *auxiliary classifiers* in the literature. In multi-exit architectures, one or more early exit *branches* are placed after some of the intermediate hidden layers of the *backbone* network. The goal of each of these branches is to provide an early result similar to the final result of the neural network using only the features extracted up to that particular branch location. These early results are inevitably less accurate than the final result of the network. In order to achieve anytime prediction using early exiting, the latest early result can be used whenever the execution is interrupted, for instance, whenever a hard deadline is reached. Computation time can be further decreased by applying model compression techniques on the backbone of multi-exit architectures. Besides anytime prediction, early exiting can also be used in *budgeted batch classification* where a fixed amount of time is available in order to classify a set of input samples. In such a setting, the result of earlier branches can be used for “easier” samples whereas the result of later branches or the final result can be used for “harder” ones. The difficulty of each sample can be determined based on the confidence of the network about its output [13], although other approaches exist in the literature [12].

Early exit branches are expected to have a low overhead in terms of the extra computation they introduce, since a high overhead would defeat the purpose. Therefore, they often contain only a handful of layers. Ideally, we want the accuracy of the early results to be close to that of the final result, since a higher accuracy for early exit branches means that the overall reliability of the system increases. However, the low-overhead constraint makes it quite challenging to achieve a high accuracy since the early exit branches have significantly

less trainable parameters compared to the rest of the network. Several approaches for increasing the accuracy of early exits such as knowledge distillation [14] and curriculum learning [15] have been suggested. In this paper, we propose a novel architecture in order to obtain more accurate early exits.

A neural architecture called *vision transformer (ViT)* [16] has been recently introduced for image classification which is radically different from convolutional neural networks. We use a modified version this architecture instead of the usual convolution and pooling layers in early exit branches and show that our method can significantly increase the accuracy of early exits compared to conventional architectures¹. The contributions of this paper can be summarized as follows:

- We propose a novel architecture for early exit branches in multi-exit architectures based on vision transformers, called *single-layer vision transformer (SL-ViT)*. We compare our method with conventional CNN-based early exit architectures across 27 scenarios involving different datasets, branch locations and backbone networks and show that our method is significantly more accurate in 26 of these scenarios, while having less overhead in terms of number of parameters and floating point operators (FLOPS). To the best of our knowledge vision transformers have never been used in multi-exit architectures before.
- We show that our method works across different modalities as well as multi-modal settings by investigating image classification, audio classification and audiovisual crowd counting scenarios. We also show that our method works for both classification and regression problems.
- We introduce a novel way of integrating audio and visual features in early exits using vision transformers. To the best of our knowledge, this is the first time early exits have been studied in multi-modal settings.
- We provide insight into why our method achieves better results compared to conventional CNN-based architectures by investigating the role of attention and receptive field.
- We introduce a fine-tuning strategy for SL-ViT called *copycat single-layer vision transformer (CC-SL-ViT)* which is based on the copycat strategy developed for CNNs [17] and show that this method can further increase the accuracy of SL-ViT early exits. To the best of our knowledge this is the first time the copycat strategy is used for vision transformers or early exits.

The rest of this paper is organized as follows: Section II provides an overview of the relevant literature; Section III describes our proposed method in detail; Section IV explains the details of our experiments; Section V showcases the experiment results; and, finally, Section VI briefly discusses the results and concludes the paper.

II. RELATED WORK

This section provides the necessary prerequisites for understanding our method and experiments. We start by describing

the particulars of multi-exit architectures. Subsequently, we provide the details of the vision transformer architecture, which is the foundation of the proposed method. Then, we briefly touch on how audio classification is normally carried out, which is included in several scenarios in our experiments. Finally, we explain another scenario investigated in our experiments, i.e. crowd counting, and how it can be approached in a multi-modal manner.

A. Multi-Exit Architectures

In order to describe multi-exit architectures, we use the same notation as Scardapane et al. [12] where a neural network is formulated as a function $f(X) = f_L(f_{L-1}(\dots f_1(X)))$. In this formulation L signifies the total number of layers in the network and f_i is the operator corresponding to layer i , which can be a convolutional layer, a fully-connected layer, a normalization layer, or any other differentiable operator. $h_i = f_i(h_{i-1})$ denotes the output of layer i , where h_0 is the input X . Finally, θ_i symbolizes the trainable parameters of layer i .

Equation (1) formulates the training process for the neural network which is achieved by tuning its parameters using an optimization algorithm on the landscape defined by a loss function. In this equation, the parameters of the neural network are denoted by $\theta = \bigcup_{i=1}^L \theta_i$, the training samples are signified by $\{(X_n, y_n)\}_{n=1}^N$, and $l(\cdot, \cdot)$ is the loss function.

$$f^* = \arg \min_{\theta} \sum_{n=1}^N l(y_n, f(X_n)) \quad (1)$$

Extending this notation to multi-exit architectures, $B \subseteq \{1, \dots, L\}$ signifies the set of selected branch locations after which early exit branches will be placed. $c_b(h_b) = y_b$ is the classifier or regressor representing the early exit branch at each branch location b , where y_b denotes the early result at that location. The schematic illustration of a multi-exit architecture is presented in Figure 1. However, since there are multiple outputs, and thus multiple loss signals in a multi-exit architecture, its training is not as straightforward.

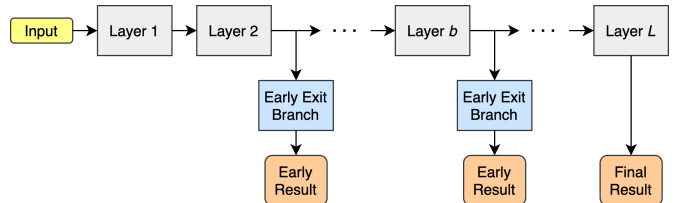


Fig. 1: Schematic illustration of a multi-exit architecture with two early exits.

Three different approaches for training multi-exit architectures exist in the literature [12], [15], [18]. In the first approach, called *end-to-end* training, the loss signals of all exits are combined and backpropagated through the network at the same time. With end-to-end training, the contribution of each loss signal to the total loss is expressed with weight values, which are therefore hyper-parameters of the model.

¹Our code will be available at https://gitlab.au.dk/maleci/sl_vit.

The second approach, called *layer-wise* training, first trains the network up to and including the first exit branch. Subsequently, the part of the network that has been trained so far is frozen, meaning its parameters are not modified any further, and the remainder of the network up to and including the second exit branch is trained. This process continues until the entire network is trained. Note that with this approach, there is no guarantee that the accuracy of the final exit remains unchanged.

In the final approach, called *classifier-wise* training, the backbone network is completely frozen and each branch is trained independent of the rest of the network and other branches, meaning the parameters θ are not modified and only the parameters of the classifiers/regressors $\{c_b\}, b \in B$ are trained. With this approach, no new hyper-parameters are introduced and the backbone remains unchanged. However, the early exit branches affect a lower number of trainable parameters compared to the other approaches.

In this paper, we choose to follow the classifier-wise training approach due to its practical importance. This is because with classifier-wise training, early exit branches can be easily added on top of existing backbone networks without the need for re-training and hyper-parameter optimization, which can be computationally expensive and time consuming. Furthermore, with end-to-end and layer-wise training strategies, the number of branches and their placement can lead to further trade-offs and affect the overall performance of the model. Since branches are independently trained in the classifier-wise strategy, any number of branches can exist and a branch can be placed at any location without affecting the performance of other branches or the backbone.

It is important to mention that branches placed later in the backbone network do not necessarily result in a higher accuracy compared to branches placed earlier. The usage of such branches would therefore not be sensible since earlier branches exist that require less computation and provide more accurate results. We hereby use the term *impractical* to refer to such branches.

B. Vision Transformer

The transformer architecture was first introduced by Vaswani et al. [19] for natural language processing, and it has recently been adapted for solving computer vision problems by Dosovitskiy et al. [16]. Vision transformer was originally developed for the problem of image classification, however, variations of vision transformer have since been applied to many computer vision problems, such as object detection, depth estimation, semantic segmentation, image generation and action recognition, as well as multi-modal data analysis tasks such as text-to-image synthesis and visual question answering [20]–[22].

In order to describe the vision transformer architecture, we first explain the *self-attention* layer. The input of this layer is in the form of a sequence $X = (x_1, \dots, x_n)$ where $X \in \mathbb{R}^{n \times d}$ and d is the embedding dimension to represent each entity. Its output is in the form of $Z = (z_1, \dots, z_n)$ where $Z \in \mathbb{R}^{n \times d_v}$. The goal of self-attention is to capture the interaction between

the entities in the sequence. For this purpose, each vector x_i in the sequence is transformed into three separate vectors: the *query* vector $q_i \in \mathbb{R}^{d_q}$, the *key* vector $k_i \in \mathbb{R}^{d_k}$ and the *value* vector $v_i \in \mathbb{R}^{d_v}$, where $d_q = d_k$. To construct the output vector z_i that corresponds to the input x_i , for each vector x_j in X (including x_i itself), the scalar a_{ij} is calculated by the inner product of q_i and k_j . Output vector z_i is then calculated by summing the value vectors v_1, \dots, v_n weighted by their corresponding scalars, that is, $z_i = \sum_{j=1}^n a_{ij} v_j$. The scalar a_{ij} basically specifies how much attention the i -th entity should pay to the j -th entity, since a_{ij} determines the contribution of v_j to the combined output z_i . In practice, the scalars are normalized by $\sqrt{d_k}$ and converted into probabilities using the softmax function.

If the key, query and value vectors are packed into matrices $Q = XW^Q$, $K = XW^K$ and $V = XW^V$, where W^Q , W^K and W^V are learnable weight matrices, the above operation can be rephrased as follows:

$$Z = \text{softmax} \left(\frac{QK^T}{\sqrt{d_k}} \right) V \quad (2)$$

In order to enable the model to capture more than one type of relationship between the entities in the sequence, self-attention is extended to *multi-head attention* by concatenating the output of h different self-attention blocks Z_1, \dots, Z_h each with its own set of learnable weight matrices, into a single matrix $Z' = [Z_0, \dots, Z_h] \in \mathbb{R}^{n \times h \cdot d_v}$, which is then projected using a weight matrix $W' \in \mathbb{R}^{h \cdot d_v \times d}$.

A *transformer encoder* is constructed by passing the input sequence into a normalization layer, a multi-head attention layer, a second normalization layer and a multi-layer perceptron (MLP), respectively. Two residual connections are added, one by adding the input sequence to the output of the multi-head attention, and the other by adding the output of the multi-head attention to the output of the MLP.

Putting it all together, a vision transformer is created by first splitting the input image into patches. Subsequently, the sequence of patches is projected into a sequence of vectors and a positional embedding is added to the corresponding vector of each patch. An additional learnable embedding called *classification token* is added to the beginning of the sequence. The sequence then passes through L transformer encoders. Finally, the first vector in the output of the last transformer encoder, which corresponds to the classification token, is passed to a MLP which outputs the final classification result. The architecture of vision transformer is depicted in Figure 2.

C. Audio Classification

Similar to image classification, audio classification is the problem of categorizing a given audio waveform into one of several predetermined classes. For instance, the given audio waveform could be a musical recording, and the goal could be to specify which genre of music it belongs to. To represent the input features, *spectrograms* obtained by applying short-time Fourier transform (STFT) and *Mel spectrograms* are commonly used [23], although raw audio waveforms can be used as well [24]. Mel spectrograms are spectrograms

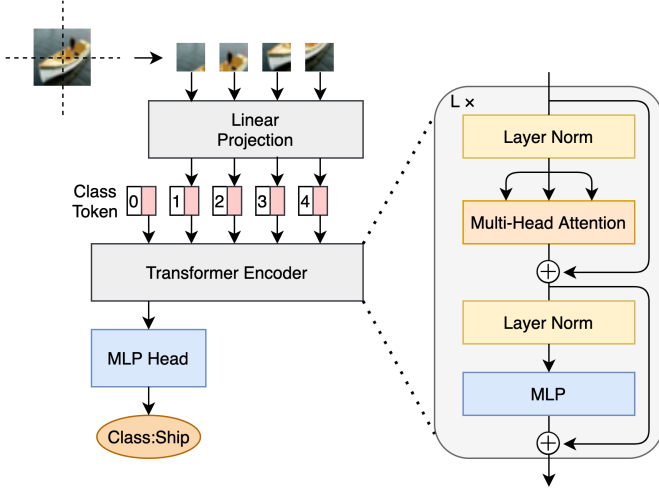


Fig. 2: The vision transformer (ViT) architecture for image classification.

that are constructed using the *Mel scale* which is a non-linear transformation of the frequency scale designed based on domain knowledge about the human auditory system. Various deep learning models for audio classification exist in the literature, including models that are commonly used for image classification, namely ResNet [25], DenseNet [26] and Inception [27], which have been shown to be quite effective for audio classification as well [28]. Conveniently, the same three networks have previously been used as backbone networks when investigating early exiting for image classification [15]. Therefore we use these backbone networks for both image and audio classification in our experiments.

D. Audiovisual Crowd Counting

Crowd counting refers to the problem of identifying the total number of people present in a given image. Crowd counting has many applications such as safety monitoring, disaster management, design of public spaces, intelligence gathering and analysis, creation of virtual environments and forensic search [29], [30]. With many of these applications, it is vital for the model to perform in near real-time. However, the input images in these scenarios often have high resolutions, such as HD or Full HD. Moreover, many of the available methods contain an immense number of parameters [31]. This means that crowd counting models are often very computationally expensive, therefore, dynamic inference methods such as early exiting and other lightweight deep learning methods become essential in real world applications.

Although the main objective of this task is to obtain a single count from an image, many methods treat this problem as dense prediction where the output is a *density map* depicting the density of the crowd across the input image, and the total count is calculated by the sum of all values in the density map. Therefore, in most crowd counting datasets, such as Shanghai Tech [32] and World Expo '10 [33], the locations of the heads of individuals in the image are annotated and provided as targets. A ground truth density map can then be obtained



Fig. 3: An example image from the Shanghai Tech dataset and its corresponding ground truth density map.

from these *head annotations* using Gaussian kernels or more complicated and specialized methods [31]. Figure 3 shows an image from the Shanghai Tech dataset and the ground truth density map that was generated from the provided head annotations using the method presented in Zhang et al [32]. In crowd counting, *Mean Absolute Error (MAE)* is usually used as a measure of accuracy whereas *Mean Squared Error (MSE)* is used as a measure of robustness [34].

Many crowd counting methods exist in the literature [31], however, most of these methods are applied in a single-modal fashion where the input is an image or a video frame. In contrast, AudioCSRNet [35], a multi-modal extension of the widely-used CSRNet model for crowd counting [36], takes as input the ambient audio of a scene in addition to its image. The authors show that the ambient audio improves the result in situations where the image quality is not ideal, for instance, low image resolution, presence of noise, occlusion and low illumination.

In CSRNet, the features extracted from the input image by the first 10 layers of a VGG-16 [37] network pre-trained on the ImageNet dataset [38] are passed through 6 dilated convolution layers and a 1×1 convolution layer in order to obtain the density map. AudioCSRNet extends this architecture by converting each of the dilated convolution layers into a fusion block. The architecture of AudioCSRNet is depicted in Figure 4. First, a Mel spectrogram is obtained from the raw audio waveform. Subsequently, in each fusion block, the features extracted from the input Mel spectrogram by the first 6 layers of a VGGish [39] network pre-trained on the AudioSet dataset [39] are projected to two vectors called γ and β which represent the multiplicative and additive aspects of the audio features. The γ and β vectors are then tiled in order to match the size of the visual features. Finally, the output of the dilated convolution is element-wise multiplied by γ and added to β .

The fusion operation can be summarized as

$$v_{l+1} = \mathcal{F}_l(\gamma_l \odot D_l(v_l) + \beta_l), \quad (3)$$

where $v_l \in \mathbb{R}^{C_l \times W_l \times H_l}$ is the output of the l -th fusion block, \mathcal{F}_l denotes an activation function, γ_l and β_l are the tiled vectors and D_l represents the l -th dilated convolution.

In practice, a batch normalization layer [40] is added immediately after each dilated convolution. Furthermore, the height and width of the intermediate features remain unchanged by using padding in the convolution operations, meaning $H_l = H_{l+1}$ and $W_l = W_{l+1}$. Additionally, since the first 10 layers of VGG-16 decrease both height and width by a

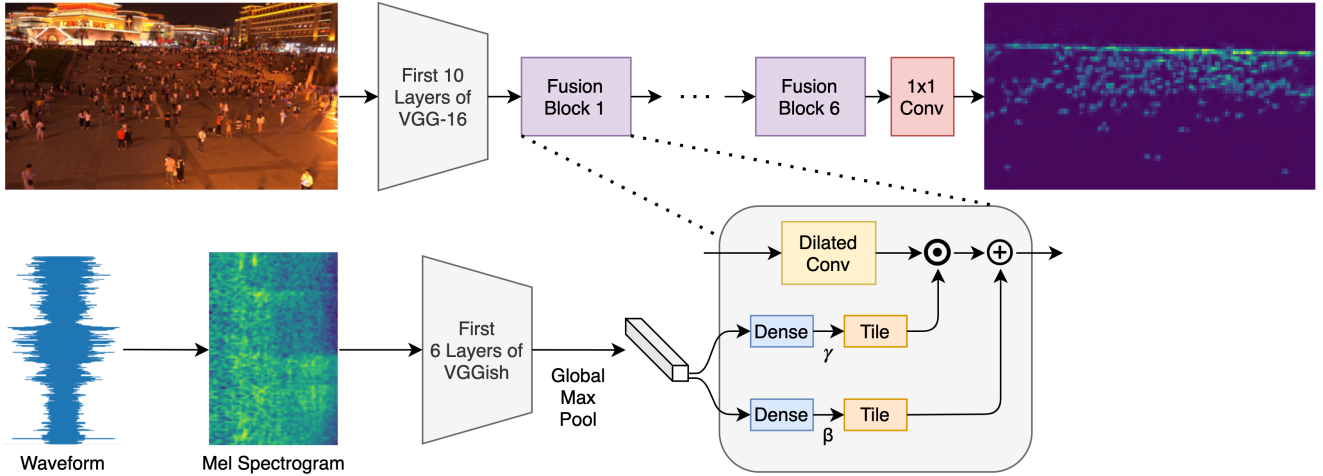


Fig. 4: Architecture of AudioCSRNet.

factor of 8 via several pooling operations, the final result of the network needs to be upsampled by a factor of 8 in order to match the resolution of the input image. It is important to preserve the total sum of the density map during this upsampling operation, since it represents the total count.

III. SINGLE-LAYER VISION TRANSFORMERS FOR EARLY EXITS

We assume a pre-trained and high performing backbone network is already available. Due to time constraints arising from the particular application, it is desirable that the network provides a result within the specific deadline rather than not providing a result at all, even though this result may be less accurate than it would be if time constraints did not exist. Therefore, the backbone needs to be augmented with early exit branches to allow for dynamic inference and anytime prediction. As previously mentioned, we use the classifier-wise approach for training the early exit branches since it results in “plug-and-play” branches that can easily be added to the backbone network without any re-training or hyper-parameter tuning.

A. *Sl-ViT*

Typically, the architecture of early exit branches starts with one or more convolution layers, although some may have no convolutions at all. Afterwards, they may have a pooling layer, which may be global pooling, and one MLP [13], [41]. Here, as a baseline, we choose to utilize the architecture depicted in Figure 5 with one 3×3 convolution, followed by a 2×2 max pooling layer and finally a MLP. The size of the max pooling layer is increased to 4×4 for crowd counting since the input images have a very high resolution. Additionally, we use dropout [42] inside the MLP to avoid overfitting. We use a single convolution since early exits with two or more convolution layers have a high overhead and may even lead to lower accuracy [13]. Early exits without convolutions are sometimes used very late in the network, however, since they are straightforward and leave no room for modifications, we do not apply our method for such cases. The resulting architecture

is a common setup within the literature, and is effectively the same architecture used for earlier exits by Hu et al. [41].

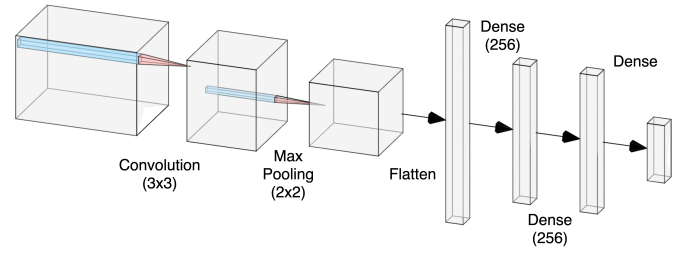


Fig. 5: Architecture of CNN early exit branches. Size of the flattened feature vector depends on the dimensions of the features at the specific branch location. For branches placed on the AudioCSRNet backbone, max pooling size is increased to 4×4 since the input images have a high resolution.²

Our method called *single-layer vision transformer* or *Sl-ViT* for short, is an alternative architecture for early exit branches that can achieve a higher accuracy compared to the aforementioned baseline, while having less overhead in terms of the number of parameters as well as floating point operations per second (FLOPS). Our proposed architecture is based on the vision transformer architecture introduced in section II-B, where instead of the input image, we split the intermediate features at the branch location into patches (sub-tensors) and pass them to a vision transformer.

However, there are some crucial differences between the original vision transformer and the architecture in our method. First, we only use a single transformer encoder layer instead of the original 12 to 36 layers, meaning that $L = 1$ in our case. Secondly, we do not utilize a separate classification token and instead pass the entire output of the transformer encoder layer to the MLP head. This is possible because both the number of patches and the size of the embedding dimension (d) in our architecture is lower than that of the original vision transformer, thus creating far less parameters when passed on to the MLP head. Variations of our architecture have 4×4 ,

²Image created using the NN-SVG tool [43].

5×5 or 8×8 patches and embedding dimensions of 32 or 36, whereas different versions of the original vision transformer have 16×16 patches and embedding dimensions of 768, 1024 or 1280. Finally, we discovered that removing the second residual connection in the transformer encoder may lead to an increase in the overall accuracy of our method. This effect was moderate in most cases, yet quite significant in others. We chose to keep the residual connection whenever the effect was moderate and only remove it if it leads to a significantly higher accuracy. Such cases are highlighted in our experiments. Our proposed architecture is shown in Figure 6. It is also important to note that the MLP head used in our architecture is exactly the same as the MLP in the CNN early exit architecture.

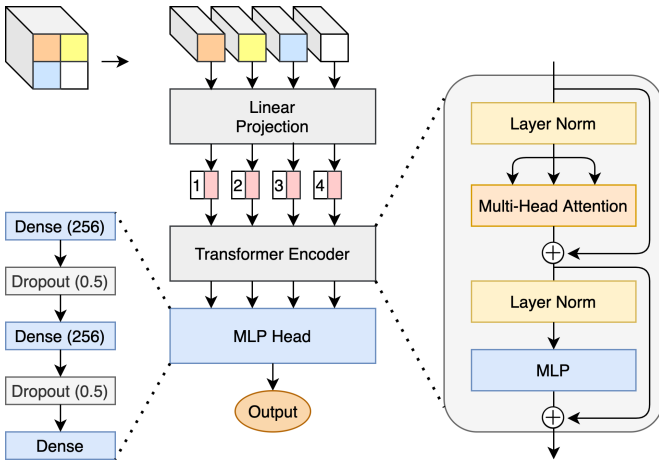


Fig. 6: Architecture of SL-ViT early exit branches. Unlike typical vision transformers, only a single transformer encoder is used, extra learnable classification token is not added to the sequence and the entire output of the transformer encoder is passed on to the MLP head. The MLP head is the same as CNN early exit branches.

Our model has several hyper-parameters, namely the size of each patch, the embedding dimension d and the number of attention heads h in multi-head attention. The patch size creates a trade-off where smaller patches result in a more fine-grained attention mechanism while increasing the total number of parameters in a bi-quadratic fashion. Therefore, similar to the original vision transformer, we choose the size of the patch to be close to the square root of the height and width of the input features. We also make sure that the size of the patch can divide the size of the input features to avoid padding, for instance, a patch size of 4×4 for input features of size 28×28 . We perform a grid search to find the values of d and h that result in the highest accuracy, while keeping the total number of parameters less than or equal to that of the CNN early exit counterpart.

At a first glance, it might seem like the SL-ViT architecture introduces more hyper-parameters than the conventional CNN architecture, however, the CNN architecture includes many design choices as well, such as the number of filters, filter size, padding, dilation, stride, pooling type and pooling size. The design choices for CNN architectures might seem simpler

since they have been studied more extensively compared to vision transformers which were introduced more recently.

B. Audiovisual SL-ViT

With audiovisual backbones such as the AudioCSRNet model for audiovisual crowd counting, described in section II-D, it is desirable to have audiovisual early exits that use both visual and audio features in order to achieve a higher accuracy. The simplest way to have such branches is to add the branches after the blocks where the fusion of visual and audio features take place. However, with our proposed SL-ViT architecture, it is also possible to include audio features as one or more patches alongside other patches, and directly fuse the features in the early exit. The advantage of this approach is that since in vision transformers, any of the patches can pay attention to any other patch, the visual features can be fused with the audio features without being directly impacted and modified. In contrast, since convolutional filters only take the immediate vicinity into account, the audio features must be present in every location. One option is to concatenate the visual features and the tiled audio features along the depth. However, that would greatly increase the amount of computation for each fusion operation, therefore intrusive operations such as element-wise multiplication and addition are used instead.

C. Copycat SL-ViT

Finally, we introduce a fine-tuning strategy for SL-ViT branches that can further increase their accuracy. Correia-Silva et al. [17] developed a method called *copycat CNN* where they create a “fake” dataset by taking images from another domain, giving them as input to a network trained on the target domain, and recording the output of the network as labels for these images. For instance, images from the ImageNet dataset [38] can be given to a network trained on the CIFAR-10 dataset [44], where the image of a camel may be labelled as a “dog” since there are no labels for “camel” in CIFAR-10. This fake dataset is then combined with a dataset for the target domain and used to train a new network. We use this strategy to fine-tune an already trained SL-ViT branch and obtain a *copycat single-layer vision transformer (CC-SL-ViT)*. Note that the ratio of the fake data mixed with the available dataset is a hyper-parameter of this fine-tuning strategy.

IV. EXPERIMENTAL SETUP

In this section, we provide the details of our experiments. We begin by giving a short summary of the datasets as well as the training details for the backbone networks. We then lay out the details of the branch architectures, their training procedure and their placement on the backbone networks, and finally explain how the copycat strategy was used to fine-tune the branches.

A total of 27 different scenarios were tested in our experiments. For both image and audio classification, two datasets, three backbone networks and two different branch locations on each backbone were tested. In addition, three different branch locations for the audiovisual crowd counting backbone

network were covered. All experiments were repeated 5 times and the average accuracy as well as the standard deviation were recorded. $4 \times$ Nvidia 2080Ti GPUs were used for the training of our models.

A. Datasets

1) *CIFAR-10 and CIFAR-100*: These are widely-used datasets for image classification [44]. Both datasets consist of 60,000 color images of size 32×32 pixels and their corresponding class labels. The images in CIFAR-10 and CIFAR-100 are categorized into 10 and 100 different classes, respectively. We use 40,000 examples for training, 10,000 for validation and another 10,000 for testing. Since our backbone networks are pre-trained on ImageNet which consists of 224×224 pixel images, we resize each image to these dimensions before passing them into the network.

2) *Speech Commands (SC)*: A well-known audio dataset of spoken words [45]. It consists of 100,503 1-second audio clips with a sampling rate of 16kHz, each labelled as one of 12 classes: 10 different spoken words such as “Yes”, “No”, “Down” and “Stop” as well as one class for background noise and another for unknown words. We use 85,511 examples for training, 10,102 for validation and 4,890 for testing. We convert the raw audio waveforms into spectrograms using short-time Fourier transform (STFT) with a window size of 255 samples and step size of 128 samples, and resize the resulting spectrograms to 224×224 before passing them into the network.

3) *GTZAN*: It is the most widely-used dataset for music genre recognition [46]. The original dataset consists of 10 genres such as “Pop” and “Rock” and 100 30-second audio clips per genre with a sampling rate of 22,050Hz. We follow the common approach to split each audio clip into 10 separate 3-second clips in order to increase the size of the dataset to 10,000. We use 8,000 examples for training, 1,000 for validation and another 1,000 for testing. Following the approach of Palanisamy et al. [28] where different spectrograms with different parameters are placed in each channel of the input image, we use one spectrogram obtained from STFT with window size of 512 samples and step size of 256 samples as well as two Mel spectrograms with 128 bins and window sizes of 100 and 50 milliseconds, and step sizes of 50 and 25 milliseconds, respectively.

4) *DISCO*: An audiovisual dataset for crowd counting which contains 1,935 images of Full HD resolution (1920×1080) [35]. For each image, a corresponding 1-second audio clip of ambient sounds with a sampling rate of 48kHz, starting 0.5 seconds before the image was taken and ending 0.5 seconds afterwards, exists as well. The labels are provided in the form of head annotations in the image. At the time of this writing, DISCO is the only publicly available dataset for audiovisual crowd counting. We use 1435 examples for training, 200 for validation and 300 for testing. The input image is resized to 1024×576 pixels to reduce memory and computation requirements. Similar to Hershey et al. [39], the input audio waveform is transformed into a Mel spectrogram with 64 bins, window size of 25 milliseconds and step size

of 10 milliseconds. Following Hu et al. [35] the ground truth density maps are obtained by convolving the head annotations with a 15×15 Gaussian kernel $\mathcal{K} \sim \mathcal{N}(0, 4.0)$.

B. Backbone networks

Transfer learning is used to train the ResNet152, DenseNet201 and InceptionV3 backbone networks for both image and audio classification. The backbone networks are all pre-trained on the ImageNet dataset and the top layer is replaced. We found that instead of adding just one dense layer at the top, as is common in transfer learning, using two dense layers and a dropout layer in between leads to a higher accuracy in our case. The resulting network is then trained using the Adam optimizer [47] with a learning rate of 10^{-4} and categorical cross-entropy loss function. The learning rate is reduced by a factor of 0.6 on plateau with a tolerance of 2 epochs, and an early stopping mechanism with a tolerance of 5 epochs is used.

The audiovisual crowd counting backbone is trained in two stages. We first train a network with the AudioCSRNet architecture described in Section II-D for 100 epochs. L_2 norm is used as loss function and AdamW [48] with a learning rate of 10^{-5} and weight decay of 10^{-4} is used as optimizer, where the learning rate is multiplied by a factor of 0.99 each epoch. This is the same training procedure used in the original paper [35]. Subsequently, in order to convert the problem from dense prediction to regression, a dense layer with an output size of one is added after the last layer of the trained AudioCSRNet. This layer is initialized as a sum, meaning the initial weights are all equal to one and no bias is used. Then the entire network is re-trained for another 100 epochs using MAE as loss function instead of the previous L_2 loss, a learning rate of 10^{-6} and weight decay of 10^{-5} . The learning rate is similarly multiplied by a factor of 0.99 every epoch. The resulting model achieves a MAE of 13.63 which is even lower than the MAE of 14.27 reported in the original paper. However, the output of the network is just a single number representing the total count instead of a density map. The final accuracy of all trained backbones can be seen in Table I.

When training the backbone networks, in order to fit the limitations of our available computational resources, the batch sizes are adjusted and some layers of the backbone networks are frozen. All backbone networks were trained with a batch size of 32 except AudioCSRNet which has a batch size of 4 as well as InceptionV3 when trained on CIFAR-10 and CIFAR-100 which has a batch size of 64. All layers of the backbone networks were trained, except in the case of ResNet152 and DenseNet201 when trained on CIFAR-10 and CIFAR-100 where only the batch normalization layers were trained. We found that training only the batch normalization layers is sufficient to achieve a high-performing backbone network in these cases [49].

C. Branches

All branches were trained using the Adam optimizer with a learning rate of 10^{-4} where the learning rate is reduced by a factor of 0.6 on plateau with a tolerance of 2 epochs,

TABLE I: Performance of backbone networks on each dataset

Backbone	CIFAR-10 Acc.	CIFAR-100 Acc.	SC Acc.	GTZAN Acc.	DISCO MAE
ResNet152	95.36%	82.25%	95.85%	91.29%	-
DenseNet201	96.48%	82.53%	96.36%	92.09%	-
InceptionV3	96.56%	83.80%	94.93%	87.79%	-
AudioCSRNet	-	-	-	-	13.63

and an early stopping mechanism with a tolerance of 5 epochs is utilized. The branches on classification backbones use a categorical cross-entropy loss function whereas the branches on the audiovisual crowd counting backbone use mean absolute error loss. The training batch size for branches were 64 in scenarios involving CIFAR-10, CIFAR-100 and Speech Commands, 32 in scenarios involving GTZAN and 4 in scenarios involving DISCO.

Table II shows the location of the branches placed on each backbone network. For the AudioCSRNet backbone network, branch V1 uses only the output of the VGG-16 layers, therefore, it only has access to the visual features. Branch AV1 uses the outputs of both VGG-16 and VGGish, therefore it has access to both audio and visual features. In this branch location, the fusion of audio and visual features is performed as described in Section III for the SL-ViT architecture, and similar to the fusion blocks in AudioCSRNet for the CNN architecture, however, without dilation. Finally, branch AV2 is placed after the first fusion block in AudioCSRNet, therefore audio and visual features have already been fused and thus fusion operation is not required within the branches. Adding branches after the second fusion block or later would not be reasonable since more than 85% of the computation of the backbone is carried out before that point, and thus the speedup resulting from early exits would be negligible.

TABLE II: Placement of branches for each backbone network

Backbone	BN*	Branch Placed After
DenseNet201	1	Transition Layer 1
	2	Transition Layer 2
ResNet152	1	12th Convolution
	2	36th Convolution
InceptionV3	1	First Filter Concat
	2	Second Filter Concat
AudioCSRNet	V1	Last Layer of VGG
	AV1	Last Layers of VGG and VGGish
	AV2	First Fusion Block

*Branch Number

D. SL-ViT and CC-SL-ViT Parameters

Table III summarizes the hyper-parameters used for the SL-ViT branches in each scenario. ‘‘Patch Size’’ shows the width and height of each image patch, ‘‘Patches’’ denotes the resulting number of patches across width and height of the input image, d is the size of embedding dimension and h is the number of heads in multi-head attention.

For copycat SL-ViT, images from the Tiny ImageNet dataset, which are the images from ImageNet down-sampled to 32×32 , were given to the InceptionV3 backbone trained on CIFAR-10, and the outputs were used to create the fake dataset. Then the fake dataset was mixed with CIFAR-10 with a 2-to-1 ratio and used for re-training.

TABLE III: Hyper-parameters of SL-ViT for different backbone networks and branches

Backbone	Dataset	BN*	Patch Size	Patches	d	h
DenseNet201	all	all	4x4	7x7	32	12
ResNet152	SC	2	4x4	7x7	32	24
	GTZAN	2	4x4	7x7	32	24
	Other		4x4	7x7	32	12
InceptionV3	CIFAR-100	all	5x5	5x5	36	8
	Other		5x5	5x5	32	12
AudioCSRNet	DISCO	all	8x8	16x9	32	12

*Branch Number

V. RESULTS

The results of our experiments are presented in Tables IV to VIII. In these Tables, the final accuracy, the total FLOPS of the model up to and including the branch and the number of parameters of just the early exit branch are compared between the CNN architecture and the SL-ViT architecture. Higher accuracies, lower errors, lower number of parameters and lower total FLOPS are highlighted in these tables. Furthermore, the speedup caused by SL-ViT early exits, defined as the total FLOPS of the backbone network divided by the total FLOPS of the model up to and including the SL-ViT branch, is also provided.

Several observations can be made about these results. First, in all scenarios except one, SL-ViT early exits achieve a significantly higher accuracy. Even in the one exceptional scenario, namely branch 2 of ResNet152 in Table VI, the accuracy of SL-ViT is very close to its CNN counterpart. Secondly, while in some cases SL-ViT branches have an equal number of parameters compared to CNN branches, in all scenarios, the total FLOPS of SL-ViT branches is lower, therefore SL-ViT branches are always more lightweight. Thirdly, in one scenario, namely branch 2 of ResNet152 in Table VII, removing the last residual connection in the SL-ViT architecture significantly improved the accuracy of the SL-ViT branch. Finally, in the AV2 branch location in Table VIII, both CNN and SL-ViT are impractical branches since earlier branches with higher accuracies exist. This is perhaps due to the intrusive fusion operation in the first fusion block which

might initially make the intermediate features more obscure. Nonetheless, even in this case, SL-ViT is more accurate.

Table IX shows the result of applying the copycat fine-tuning strategy to SL-ViT branches for the CIFAR-10 dataset. Observe that in all cases, the accuracy is significantly increased compared to SL-ViT, which itself was more accurate than CNN based on Table IV. We also tested this strategy for the CIFAR-100 dataset with 10-to-1, 2-to-1 and 1-to-1 ratios of fake and real data, however, neither improved the overall accuracy. Perhaps another mixing ratio, choice of dataset and network to generate the fake dataset, optimizer or hyper-parameters such as learning rate may result in improvements for CIFAR-100.

Finally, Table X showcases the effect of increasing the number of attention heads in multi-head attention for the specific scenario involving branch 1 of ResNet152 backbone on CIFAR-10 dataset. Note that with each increase in the number of attention heads in SL-ViT, while the number of branch parameters is only slightly increased and still much lower than that of CNN, the jump in accuracy is quite significant until it plateaus at 12 heads.

VI. DISCUSSION AND CONCLUSION

We showed that the proposed architecture for early exit branches, namely single-layer vision transformer (SL-ViT) can consistently obtain a significantly higher accuracy compared to conventional methods while introducing a lower overhead in terms of FLOPS. We showed that our method works for both classification and regression problems, in both single and multi-modal scenarios, and across different backbone networks and branch locations.

One possible explanation for why SL-ViT performs better, is the fact that even a single layer of transformer encoder has a global receptive field since each patch can attend to any other patch, while a convolutional layer has a limited receptive field and can only access the immediate vicinity based on its filter size. There are several clues that point to this explanation. First, Table X suggests that the attention mechanism plays a major role in the accuracy improvements. Secondly, based on Tables IV to VIII, the accuracy improvements are generally higher in earlier branches, where the receptive field of the backbone network up to the branch location is lower compared to later branches. Finally, the incorporation of global scale and global information such as perspective is known to be of great importance in crowd counting, and many crowd counting methods utilize visual attention mechanisms and dilation convolution layers to this end [31], which can explain why our method performs well for this problem.

Moreover, we showed that our fine-tuning strategy, namely Copycat SL-ViT, has the potential to further increase the accuracy of SL-ViT branches. It is well-known that with deep learning, more data almost always improves the final outcome, and this is especially true for vision transformers which are known to be data-hungry [21]. The copycat strategy can at times artificially increase the size of the dataset without introducing too much noise and thus improve the final result.

Furthermore, we introduced a novel approach for fusing audio and visual features within early exits using vision

transformers. The importance of fusion inside early exits is that it creates much more options for branch locations, since a combination of any layer in the visual channel of the backbone network with any layer in the audio channel of the backbone can be selected. This allows for a more fine-grained dynamic inference, meaning a more recent result is available whenever the inference is interrupted in an anytime prediction setting, which is likely to be more accurate than earlier results.

REFERENCES

- [1] Y. LeCun, Y. Bengio, and G. Hinton, "Deep learning," *Nature*, vol. 521, no. 7553, pp. 436–444, May 2015. [Online]. Available: <https://doi.org/10.1038/nature14539>
- [2] Y. Cheng, D. Wang, P. Zhou, and T. Zhang, "Model compression and acceleration for deep neural networks: The principles, progress, and challenges," *IEEE Signal Processing Magazine*, vol. 35, no. 1, pp. 126–136, Jan. 2018. [Online]. Available: <https://doi.org/10.1109/psmp.2017.2765695>
- [3] M. Rastegari, V. Ordonez, J. Redmon, and A. Farhadi, "XNOR-net: ImageNet classification using binary convolutional neural networks," in *Computer Vision – ECCV 2016*. Springer International Publishing, 2016, pp. 525–542. [Online]. Available: https://doi.org/10.1007/978-3-319-46493-0_32
- [4] H. Li, A. Kadav, I. Durdanovic, H. Samet, and H. P. Graf, "Pruning filters for efficient convnets," 2016.
- [5] D. T. Tran, A. Iosifidis, and M. Gabbouj, "Improving efficiency in convolutional neural network with multilinear filters," *Neural Networks*, vol. 105, pp. 328–339, 2018.
- [6] G. Hinton, O. Vinyals, and J. Dean, "Distilling the knowledge in a neural network," 2015.
- [7] H. Zhao, X. Sun, J. Dong, C. Chen, and Z. Dong, "Highlight every step: Knowledge distillation via collaborative teaching," *IEEE Transactions on Cybernetics*, pp. 1–12, 2020.
- [8] J. Chen and X. Ran, "Deep learning with edge computing: A review," *Proceedings of the IEEE*, vol. 107, no. 8, pp. 1655–1674, Aug. 2019. [Online]. Available: <https://doi.org/10.1109/jproc.2019.2921977>
- [9] X. Wang, Y. Han, V. C. M. Leung, D. Niyato, X. Yan, and X. Chen, "Convergence of edge computing and deep learning: A comprehensive survey," *IEEE Communications Surveys & Tutorials*, vol. 22, no. 2, pp. 869–904, 2020. [Online]. Available: <https://doi.org/10.1109/comst.2020.2970550>
- [10] L. Vu, V. L. Cao, Q. U. Nguyen, D. N. Nguyen, D. T. Hoang, and E. Dutkiewicz, "Learning latent representation for iot anomaly detection," *IEEE Transactions on Cybernetics*, pp. 1–14, 2020.
- [11] Y. Han, G. Huang, S. Song, L. Yang, H. Wang, and Y. Wang, "Dynamic neural networks: A survey," 2021.
- [12] S. Scardapane, M. Scarpiniti, E. Baccarelli, and A. Uncini, "Why should we add early exits to neural networks?" *Cognitive Computation*, vol. 12, no. 5, pp. 954–966, Jun. 2020. [Online]. Available: <https://doi.org/10.1007/s12559-020-09734-4>
- [13] S. Teerapittayanon, B. McDanel, and H. Kung, "BranchyNet: Fast inference via early exiting from deep neural networks," in *2016 23rd International Conference on Pattern Recognition (ICPR)*. IEEE, Dec. 2016. [Online]. Available: <https://doi.org/10.1109/icpr.2016.7900006>
- [14] M. Phuong and C. Lampert, "Distillation-based training for multi-exit architectures," in *2019 IEEE/CVF International Conference on Computer Vision (ICCV)*. IEEE, Oct. 2019. [Online]. Available: <https://doi.org/10.1109/iccv.2019.00144>
- [15] A. Bakhtiarnia, Q. Zhang, and A. Iosifidis, "Improving the accuracy of early exits in multi-exit architectures via curriculum learning," 2021.
- [16] A. Dosovitskiy, L. Beyer, A. Kolesnikov, D. Weissenborn, X. Zhai, T. Unterthiner, M. Dehghani, M. Minderer, G. Heigold, S. Gelly, J. Uszkoreit, and N. Houlsby, "An image is worth 16x16 words: Transformers for image recognition at scale," in *International Conference on Learning Representations*, 2021. [Online]. Available: <https://openreview.net/forum?id=YicbFdNTTy>
- [17] J. R. Correia-Silva, R. F. Berriel, C. Badue, A. F. de Souza, and T. Oliveira-Santos, "Copycat CNN: Stealing knowledge by persuading confession with random non-labeled data," in *2018 International Joint Conference on Neural Networks (IJCNN)*. IEEE, Jul. 2018. [Online]. Available: <https://doi.org/10.1109/ijcnn.2018.8489592>

TABLE IV: Comparison of different early exit architectures on the CIFAR-10 dataset

Backbone	Branch	Accuracy		Branch Params		Total FLOPS		Speedup SL-ViT
		CNN	SL-ViT	CNN	SL-ViT	CNN	SL-ViT	
ResNet152	1	66.78 ± 0.57%	71.06 ± 0.55%	0.78M	0.59M	1.66B	1.64B	13.77
	2	79.31 ± 0.81%	81.18 ± 0.52%	0.83M	0.79M	5.33B	5.26B	4.29
DenseNet201	1	71.27 ± 0.36%	76.38 ± 0.33%	0.78M	0.59M	2.55B	2.53B	3.39
	2	80.64 ± 0.29%	83.53 ± 0.37%	0.80M	0.66M	4.21B	4.17B	2.06
InceptionV3	1	77.27 ± 0.58%	79.99 ± 0.20%	0.61M	0.56M	2.17B	2.14B	2.65
	2	79.55 ± 0.24%	81.72 ± 0.53%	0.61M	0.56M	2.53B	2.49B	2.28

TABLE V: Comparison of different early exit architectures on the CIFAR-100 dataset

Backbone	Branch	Accuracy		Branch Params		Total FLOPS		Speedup SL-ViT
		CNN	SL-ViT	CNN	SL-ViT	CNN	SL-ViT	
ResNet152	1	34.93 ± 0.52%	38.59 ± 1.40%	0.80M	0.61M	1.66B	1.64B	13.77
	2	47.39 ± 0.65%	53.93 ± 0.68%	0.86M	0.81M	5.33B	5.26B	4.29
DenseNet201	1	33.91 ± 1.00%	42.50 ± 0.69%	0.80M	0.61M	2.55B	2.53B	3.39
	2	47.22 ± 0.45%	50.76 ± 1.01%	0.82M	0.68M	4.21B	4.17B	2.06
InceptionV3	1	43.18 ± 0.69%	46.86 ± 0.57%	0.63M	0.63M	2.17B	2.14B	2.66
	2	44.87 ± 0.83%	49.07 ± 0.55%	0.63M	0.63M	2.53B	2.50B	2.28

TABLE VI: Comparison of different early exit architectures on the Speech Commands dataset

Backbone	Branch	Accuracy		Branch Params		Total FLOPS		Speedup SL-ViT
		CNN	SL-ViT	CNN	SL-ViT	CNN	SL-ViT	
ResNet152	1	75.80 ± 0.73%	84.05 ± 0.31%	0.78M	0.59M	1.66B	1.64B	13.77
	2	89.78 ± 0.24%	89.63 ± 0.52%	0.84M	0.84M	5.33B	5.26B	4.29
DenseNet201	1	72.78 ± 0.64%	87.94 ± 0.85%	0.78M	0.59M	2.55B	2.53B	3.39
	2	86.56 ± 0.61%	90.93 ± 0.52%	0.80M	0.66M	4.21B	4.17B	2.06
InceptionV3	1	84.64 ± 0.88%	87.62 ± 0.65%	0.61M	0.56M	2.17B	2.14B	2.65
	2	87.08 ± 1.11%	88.33 ± 0.92%	0.61M	0.56M	2.53B	2.49B	2.28

TABLE VII: Comparison of different early exit architectures on the GTZAN dataset

Backbone	Branch	Accuracy		Branch Params		Total FLOPS		Speedup SL-ViT
		CNN	SL-ViT	CNN	SL-ViT	CNN	SL-ViT	
ResNet152	1	67.01 ± 1.11%	73.27 ± 0.91%	0.78M	0.59M	1.66B	1.64B	13.77
	2*	80.26 ± 2.07%	81.56 ± 1.57%	0.83M	0.83M	5.33B	5.26B	4.29
DenseNet201	1	70.65 ± 1.23%	76.38 ± 1.94%	0.78M	0.59M	2.55B	2.53B	3.39
	2	81.72 ± 0.62%	84.00 ± 1.67%	0.80M	0.66M	4.21B	4.17B	2.06
InceptionV3	1	77.86 ± 0.90%	79.42 ± 0.99%	0.61M	0.56M	2.17B	2.14B	2.65
	2	78.90 ± 0.90%	79.90 ± 0.79%	0.61M	0.56M	2.53B	2.49B	2.28

*The last residual connection in the SL-ViT architecture was removed in this case

TABLE VIII: Comparison of Different Early Exit Architectures on the DISCO Dataset

Backbone	Branch	MAE		Branch Params		Total FLOPS		Speedup SL-ViT
		CNN	SL-ViT	CNN	SL-ViT	CNN	SL-ViT	
AudioCSRNet	V1	16.99 ± 0.28	15.04 ± 0.71	2.50M	2.35M	329.77B	328.72B	1.49
	AV1	17.00 ± 0.23	14.58 ± 0.64	2.52M	2.36M	331.37B	330.31B	1.48
	AV2	17.90 ± 0.25	17.03 ± 1.04	2.50M	2.35M	374.86B	373.81B	1.31

TABLE IX: Effect of Copycat strategy demonstrated on the CIFAR-10 dataset

Backbone	Branch	Accuracy	
		SL-ViT	CC-SL-ViT
ResNet152	1	71.06 ± 0.55%	71.61 ± 0.45%
	2	81.18 ± 0.52%	83.41 ± 0.15%
DenseNet201	1	76.38 ± 0.33%	78.34 ± 0.31%
	2	83.53 ± 0.37%	84.89 ± 0.43%
InceptionV3	1	79.99 ± 0.20%	80.78 ± 0.23%
	2	81.72 ± 0.53%	82.20 ± 0.40%

TABLE X: Effect of increasing the number of attention heads for the case of ResNet152 backbone network, CIFAR-10 dataset and first branch location

Architecture	Heads	Accuracy	Branch Params
SL-ViT	4	69.15%	0.55M
	8	70.42%	0.57M
	12	71.28%	0.59M
	16	71.24%	0.60M
CNN	-	66.62%	0.78M

- [18] E. Baccarelli, S. Scardapane, M. Scarpiniti, A. Momenzadeh, and A. Uncini, "Optimized training and scalable implementation of conditional deep neural networks with early exits for fog-supported IoT applications," *Information Sciences*, vol. 521, pp. 107–143, Jun. 2020. [Online]. Available: <https://doi.org/10.1016/j.ins.2020.02.041>
- [19] A. Vaswani, N. Shazeer, N. Parmar, J. Uszkoreit, L. Jones, A. N. Gomez, L. u. Kaiser, and I. Polosukhin, "Attention is all you need," in *Advances in Neural Information Processing Systems*, I. Guyon, U. V. Luxburg, S. Bengio, H. Wallach, R. Fergus, S. Vishwanathan, and R. Garnett, Eds., vol. 30. Curran Associates, Inc., 2017. [Online]. Available: <https://proceedings.neurips.cc/paper/2017/file/3f5ee243547dee91fbd053c1c4a845aa-Paper.pdf>
- [20] K. Han, Y. Wang, H. Chen, X. Chen, J. Guo, Z. Liu, Y. Tang, A. Xiao, C. Xu, Y. Xu, Z. Yang, Y. Zhang, and D. Tao, "A survey on visual transformer," 2020.
- [21] S. Khan, M. Naseer, M. Hayat, S. W. Zamir, F. S. Khan, and M. Shah, "Transformers in vision: A survey," 2021.
- [22] S. F. Bhat, I. Alhashim, and P. Wonka, "Adabins: Depth estimation using adaptive bins," 2020.
- [23] K. Choi, G. Fazekas, and M. Sandler, "Automatic tagging using deep convolutional neural networks," 2016.
- [24] J. Lee, T. Kim, J. Park, and J. Nam, "Raw waveform-based audio classification using sample-level cnn architectures," 2017.
- [25] K. He, X. Zhang, S. Ren, and J. Sun, "Deep residual learning for image recognition," in *2016 IEEE Conference on Computer Vision and Pattern Recognition (CVPR)*. IEEE, Jun. 2016. [Online]. Available: <https://doi.org/10.1109/cvpr.2016.90>
- [26] G. Huang, Z. Liu, L. V. D. Maaten, and K. Q. Weinberger, "Densely connected convolutional networks," in *2017 IEEE Conference on Computer Vision and Pattern Recognition (CVPR)*. IEEE, Jul. 2017. [Online]. Available: <https://doi.org/10.1109/cvpr.2017.243>
- [27] C. Szegedy, V. Vanhoucke, S. Ioffe, J. Shlens, and Z. Wojna, "Rethinking the inception architecture for computer vision," in *2016 IEEE Conference on Computer Vision and Pattern Recognition (CVPR)*. IEEE, Jun. 2016. [Online]. Available: <https://doi.org/10.1109/cvpr.2016.308>
- [28] K. Palanisamy, D. Singhania, and A. Yao, "Rethinking cnn models for audio classification," 2020.
- [29] V. A. Sindagi and V. M. Patel, "A survey of recent advances in CNN-based single image crowd counting and density estimation," *Pattern Recognition Letters*, vol. 107, pp. 3–16, May 2018. [Online]. Available: <https://doi.org/10.1016/j.patrec.2017.07.007>
- [30] Q. Wang, W. Lin, J. Gao, and X. Li, "Density-aware curriculum learning for crowd counting," *IEEE Transactions on Cybernetics*, pp. 1–13, 2020.
- [31] G. Gao, J. Gao, Q. Liu, Q. Wang, and Y. Wang, "Cnn-based density estimation and crowd counting: A survey," 2020.
- [32] Y. Zhang, D. Zhou, S. Chen, S. Gao, and Y. Ma, "Single-image crowd counting via multi-column convolutional neural network," in *2016 IEEE Conference on Computer Vision and Pattern Recognition (CVPR)*. IEEE, Jun. 2016. [Online]. Available: <https://doi.org/10.1109/cvpr.2016.70>
- [33] C. Zhang, H. Li, X. Wang, and X. Yang, "Cross-scene crowd counting via deep convolutional neural networks," in *2015 IEEE Conference on Computer Vision and Pattern Recognition (CVPR)*. IEEE, Jun. 2015. [Online]. Available: <https://doi.org/10.1109/cvpr.2015.7298684>
- [34] F. Dai, H. Liu, Y. Ma, J. Cao, Q. Zhao, and Y. Zhang, "Dense scale network for crowd counting," 2019.
- [35] D. Hu, L. Mou, Q. Wang, J. Gao, Y. Hua, D. Dou, and X. X. Zhu, "Ambient sound helps: Audiovisual crowd counting in extreme conditions," 2020.
- [36] Y. Li, X. Zhang, and D. Chen, "CSRNet: Dilated convolutional neural networks for understanding the highly congested scenes," in *2018 IEEE/CVF Conference on Computer Vision and Pattern Recognition*. IEEE, Jun. 2018. [Online]. Available: <https://doi.org/10.1109/cvpr.2018.00120>
- [37] K. Simonyan and A. Zisserman, "Very deep convolutional networks for large-scale image recognition," in *3rd International Conference on Learning Representations, ICLR 2015, San Diego, CA, USA, May 7-9, 2015, Conference Track Proceedings*, Y. Bengio and Y. LeCun, Eds., 2015. [Online]. Available: <http://arxiv.org/abs/1409.1556>
- [38] J. Deng, W. Dong, R. Socher, L.-J. Li, K. Li, and L. Fei-Fei, "ImageNet: A large-scale hierarchical image database," in *2009 IEEE Conference on Computer Vision and Pattern Recognition*. IEEE, Jun. 2009. [Online]. Available: <https://doi.org/10.1109/cvpr.2009.5206848>
- [39] S. Hershey, S. Chaudhuri, D. P. W. Ellis, J. F. Gemmeke, A. Jansen, R. C. Moore, M. Plakal, D. Platt, R. A. Saurous, B. Seybold, M. Slaney, R. J. Weiss, and K. Wilson, "CNN architectures for large-scale audio classification," in *2017 IEEE International Conference on Acoustics, Speech and Signal Processing (ICASSP)*. IEEE, Mar. 2017. [Online]. Available: <https://doi.org/10.1109/icassp.2017.7952132>
- [40] S. Ioffe and C. Szegedy, "Batch normalization: Accelerating deep network training by reducing internal covariate shift," in *Proceedings of the 32nd International Conference on Machine Learning*, ser. Proceedings of Machine Learning Research, F. Bach and D. Blei, Eds., vol. 37. Lille, France: PMLR, 07–09 Jul 2015, pp. 448–456. [Online]. Available: <http://proceedings.mlr.press/v37/ioffe15.html>
- [41] T. Hu, T. Chen, H. Wang, and Z. Wang, "Triple wins: Boosting accuracy, robustness and efficiency together by enabling input-adaptive inference," in *ICLR*, 2020.
- [42] N. Srivastava, G. Hinton, A. Krizhevsky, I. Sutskever, and R. Salakhutdinov, "Dropout: A simple way to prevent neural networks from overfitting," *J. Mach. Learn. Res.*, vol. 15, no. 1, p. 1929–1958, Jan. 2014.
- [43] A. LeNail, "NN-SVG: Publication-ready neural network architecture schematics," *Journal of Open Source Software*, vol. 4, no. 33, p. 747, Jan. 2019. [Online]. Available: <https://doi.org/10.21105/joss.00747>
- [44] A. Krizhevsky, "Learning multiple layers of features from tiny images," 2009.
- [45] P. Warden, "Speech commands: A dataset for limited-vocabulary speech recognition," 2018.
- [46] G. Tzanetakis and P. Cook, "Musical genre classification of audio signals," *IEEE Transactions on Speech and Audio Processing*, vol. 10, no. 5, pp. 293–302, Jul. 2002. [Online]. Available: <https://doi.org/10.1109/tsa.2002.800560>
- [47] D. P. Kingma and J. Ba, "Adam: A method for stochastic optimization," in *3rd International Conference on Learning Representations, ICLR 2015, San Diego, CA, USA, May 7-9, 2015, Conference Track Proceedings*, Y. Bengio and Y. LeCun, Eds., 2015. [Online]. Available: <http://arxiv.org/abs/1412.6980>
- [48] I. Loshchilov and F. Hutter, "Decoupled weight decay regularization," in *7th International Conference on Learning Representations, ICLR 2019, New Orleans, LA, USA, May 6-9, 2019*. OpenReview.net, 2019. [Online]. Available: <https://openreview.net/forum?id=Bkg6RiCqY7>
- [49] J. Frankle, D. J. Schwab, and A. S. Morcos, "Training batchnorm and only batchnorm: On the expressive power of random features in cnns," 2020.